Journal of Hazardous Materials 402 (2021) 123531

Contents lists available at ScienceDirect

Journal of Hazardous Materials

journal homepage: www.elsevier.com/locate/jhazmat

An ultrasensitive platform for PCB77 detection: New strategy for liquid crystal-based aptasensor fabrication

Asma Verdian*, Zeinab Rouhbakhsh, Ebrahim Fooladi

Department of Food Safety and Quality Control, Research Institute of Food Science and Technology (RIFST), Mashhad, Iran

GRAPHICAL ABSTRACT

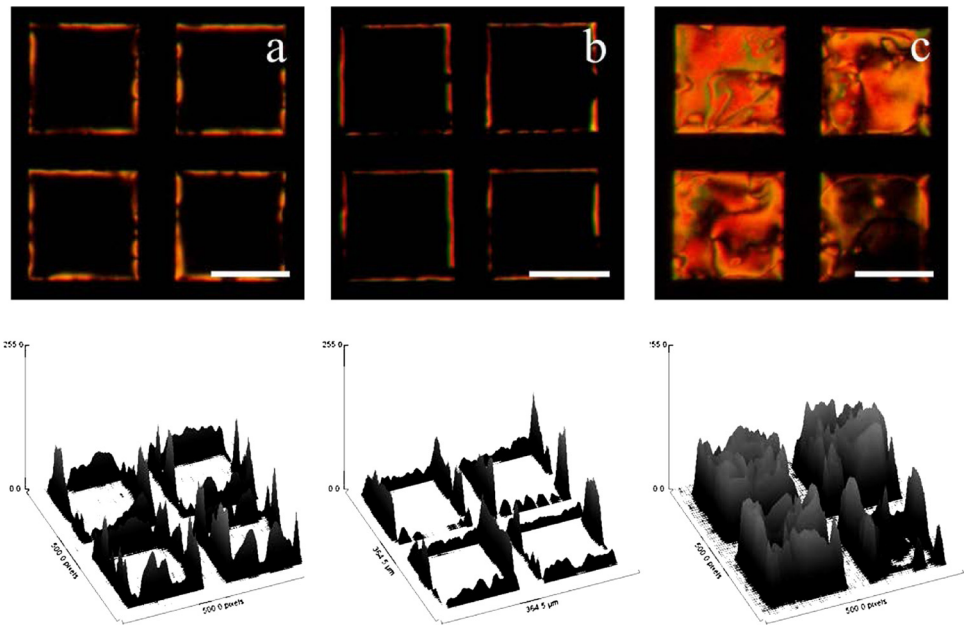

ARTICLE INFO

Editor: D. Aga

Keywords:
Polychlorinated biphenyls
Liquid crystals
Biosensor
Aptamer
Polarized light microscopy

ABSTRACT

Polychlorinated biphenyls (PCBs) are considered persistent bio-accumulative toxicants which threats global food safety and environmental health. Traditional analytical techniques for detection of PCBs are time-consuming and they do not satisfy urgent need for rapid and accurate monitoring of these persistent pollutants. Biosensor technology may be promising in this respect. Here we demonstrate a novel liquid crystal (LC)-based aptasensing platform as a promising label-free and rapid biosensor for PCB77 detection. This novel molecular strategy utilize triple-helix molecular conformational switch which is mediated formation of duplex on sensing platform in presence of target. Duplex forming leads to optical change from dark to bright in a liquid crystal based aptasensor. The limit of quantification of the LC-aptasensor to PCB77 is 1.5 × 10^{-5} μg/L with comparable selectivity. Besides, we also demonstrated that this system is able to detect PCB77 in tap water, environmental

* Corresponding author.
E-mail address: a.verdian@rifst.ac.ir (A. Verdian).

https://doi.org/10.1016/j.jhazmat.2020.123531
Received 28 January 2020; Received in revised form 10 July 2020; Accepted 17 July 2020
Available online 23 July 2020

water and milk. This strategy has potential for label-free and portable detection of different targets without any aptamer sequence length restrictions.

1. Introduction

Polychlorinated biphenyls (PCBs) are a toxic class of man-made chemicals from persistent organic pollutants (Safe, 1994). PCBs as lipophilic pollutants accumulate in mammal fat tissues and their increasing levels threat food safety and human health (Carpenter, 2006; Robertson and Hansen, 2015). Their production and usage in industrial processes have been banned since the 1970s due to the highly irreparably effects of PCBs on humans such as carcinogenicity, mutagenicity, an endocrine disorder, and thyroid dysfunction (Choi et al., 2004; Knerr and Schrenk, 2006). PCBs as an ecosystem threat could remain persistence in the environment for long periods of time, and then get taken in the food chain. The present of different micro-pollutants in the water is a global concern (Alver and Baştürk, 2019; Argun et al., 2017; Alver and Kılıç, 2018; Alver et al., 2018). The maximum level of 0.5 μg/L of contaminant PCBs in the drinking has regulated by the Environmental Protection Agency (EPA) (Ahmad et al., 2019). Monitoring of PCBs in food and environment is the most efficient approach to evaluate the risk of human exposure. The coplanar PCBs such as PCB77 (structure in Fig. S1) among 209 congeners are the most toxic dioxin-like chemicals (Chiu et al., 2001). The traditional PCBs detection methods for the quantification of PCBs in suspected samples are often gas chromatography-mass spectrometry (GC–MS) and high-performance liquid chromatography-mass spectrometry (HPLC-MS) (Ozcan et al., 2009; Berger et al., 2004; Zhang et al., 2016). However, they are very expensive, time-consuming, and need the exhausting pre-treatment process with hiring a specialized technician. The biosensor technology as a simple, rapid, affordable, portable, and user-friend tools is a promising strategy to solve such problems (Verdian, 2018). At the moment, ELISA commercial kits which validated by the U.S. EPA are available (Chiu et al., 2001; Verdian et al., 2019). However, antibodies as the recognition elements in ELISA commercial kits have several limitations in terms of stability, screening cost, and production time (Javidi et al., 2018). Recently, aptamers as proper alternatives have been attending for detection assays. Aptamers have many advantages, such as high affinity and specificity, cost-effectiveness, better target versatility, reusability, low immunogenicity, and faster synthesis compared to antibodies (Khoshbin et al., 2019, 2018). In the past decade, publications have reported the selection of novel DNA aptamers for the binding to PCBs (Verdian et al., 2019; Mehta et al., 2012). Researchers' attention about the next generation of the biosensors, moved to portable devices and point of care (POC) market (Zarei, 2017). The appearance of liquid crystals (LCs) biosensors as a promise POC device opened a new perspective and opportunities for scientists (Popov et al., 2017; Hussain et al., 2016). LCs-based biosensors can be portable through smartphone-integrated microscopies (Nandi and Pal, 2018). These soft materials with fluidity and long-range order in orientation have properties intermediate between solid and liquid. LCs with very low anchoring energy that makes them very sensitive to external stimuli are responsive materials to any nano-scale interfacial interactions based on the change of orientation LC mesogens. Since, LCs are birefringent materials, the polarizing microscopy with a vicinity molecular occurring takes distinctive optical images. In addition, LC-biosensors are label-free, high sensitive and selective assays for the detection of analytes without using bulky and expensive instrumentation (Yang et al., 2012; Tan et al., 2014). Therefore, LC-aptasensors have been applied for the detection of some analytes in over a decade (Kim et al., 2018; Kim and Jang, 2019; Wang et al., 2017; Qi et al., 2019; Ren et al., 2019; Du et al., 2019; Clemente et al., 2019; Rouhbakhsh et al., 2020).

The LCs orientational order is very sensitive to the chemical and physical properties of the surfaces. Therefore, a suitable pre-treatment of the substrate surfaces is necessary for LC-based sensors. On the basis of previous observations, there is a restriction regarding the LC orientation behavior on the substrate surface-immobilized with ssDNA oligonucleotides (Steel et al., 2000; Shen et al., 2017). The LCs orientational order in the mesophase can easily disrupt when the aptamer strands are longer than 24 bases and the longer sequence takes a random curly state (Steel et al., 2000). To address the above-mentioned issues, we introduced a novel molecular engineering strategy for the development of a universal and convenient LC-based sensing platform for the long-sequence aptamers based on a well-known triple-helix molecular switch (THMS) structure (Zheng et al., 2011; Bagheri et al.,

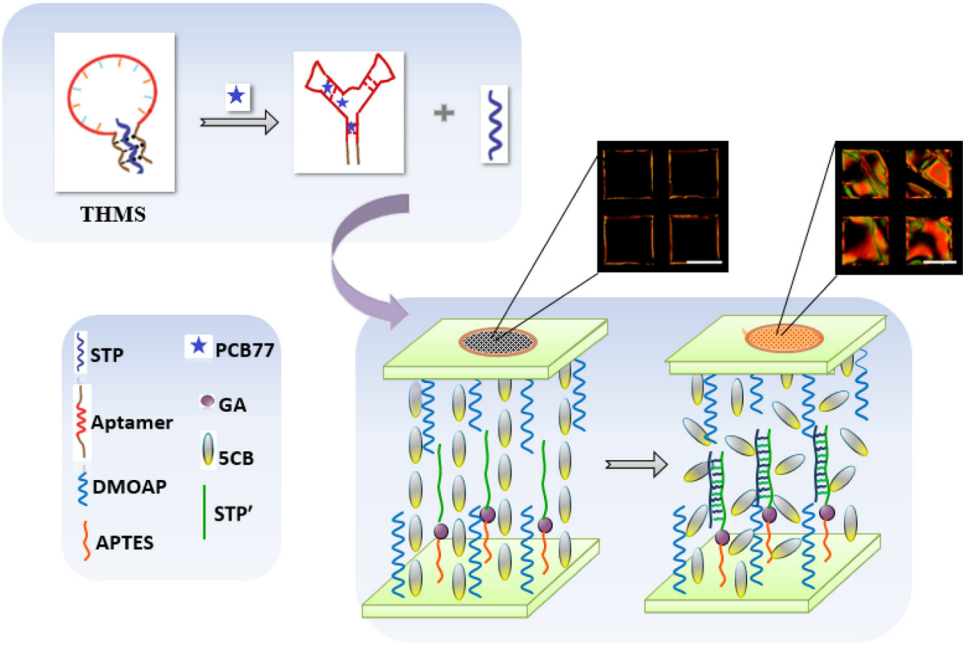

Scheme 1. The schematic diagram of the aptamer-based LC biosensor for PCB77. After the aptamer binding with PCB77, the structure of THMS is disassembled and liberated STP bind to the STP′ on LC-cell. Duplex forming on the LC cell considerably disrupts the homeotropic alignments of LCs. The corresponding optical responses associated with this orientation switch of LCs from dark to bright appearances. (For interpretation of the references to colour in this Scheme text, the reader is referred to the web version of this article.)

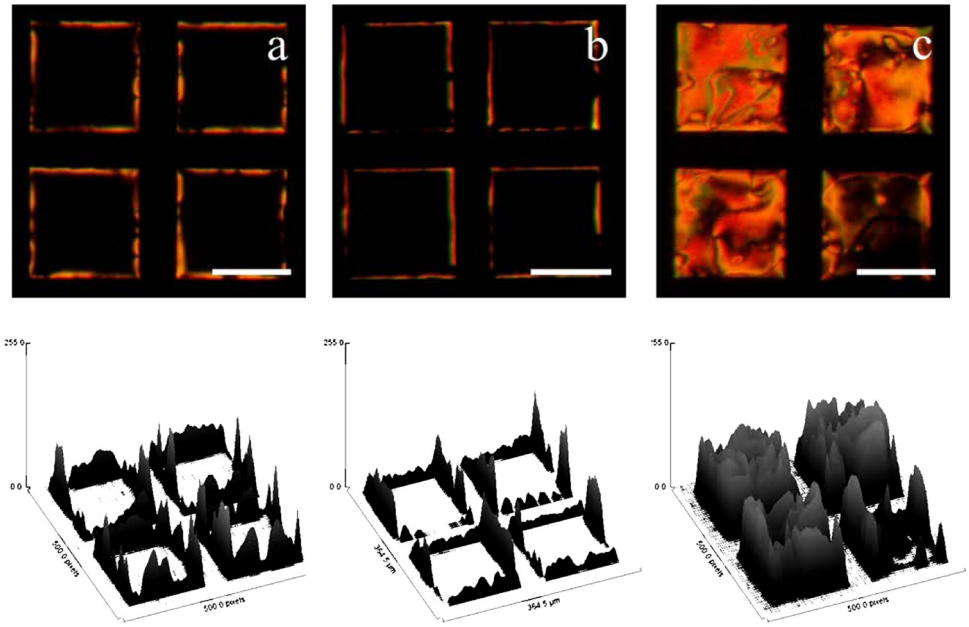

Fig. 1. Optical appearances and corresponding surface plot of the LC cells under crossed polarizers with (a) 100 nM STP′; (b) 150 nM THMS in the absence of PCB77; (c) 150 nM THMS in the presence of 1.5 μg/L PCB77.

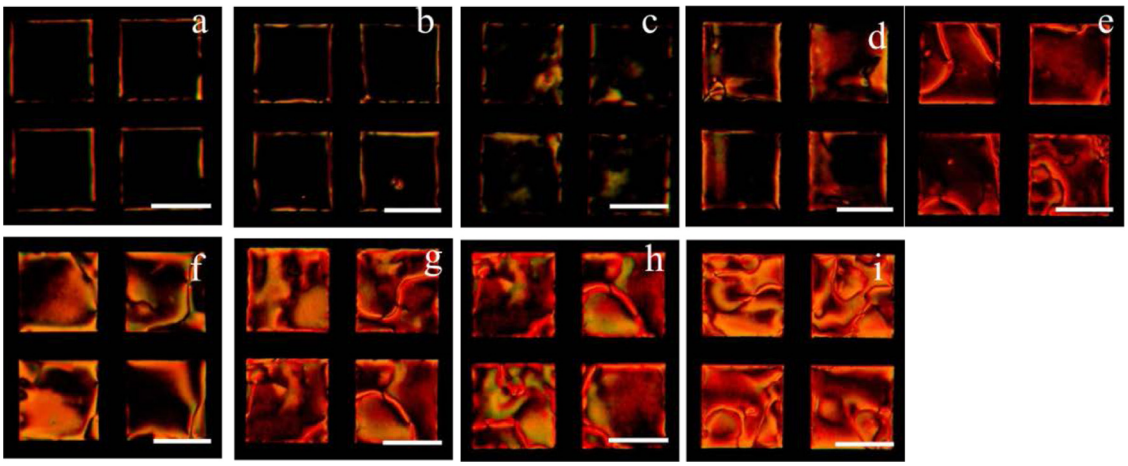

Fig. 2. Optical appearances of the LC cells under crossed polarizers of different concentration of PCB77: (a) 0 μg/L; (b) 1.5×10^{-5} μg/L; (c) 0.3×10^{-4} μg/L; (d) 0.3×10^{-3} μg/L; (e) 0.3×10^{-2} μg/L; (f) 0.3×10^{-1} μg/L; (g) 0.3 μg/L; (h) 1.5 μg/L and (i) 15 μg/L.

2018; Verdian et al., 2014). We choose PCB77 aptamer as a proof-of-concept model and design a displacement-based strategy. Compared to the known molecular switch strategies, the THMS possesses several unique characteristics such as, high stability, selectivity and affinity of the original aptamer. It is a label-free strategy and above all, this strategy is generalizable namely, just an signal transduction probe (STP) used for the detection of the multiplicate target by selecting different types of aptamers (Zheng et al., 2011; Hu et al., 2020). Therefore, this approach is not only highly sensitive and selective but also generalizable and convenient which decreases the complexity and cost of the STP synthesis. In the developed LC-based biosensor, a short sequence as STP′ immobilized on the surface of glass slide which induces a homeotropic orientation of LCs with a dark background. STP′ is a complementary sequence of signal transduction probe (STP) in THMS structure. The binding of aptamer and PCB77 breaks down the THMS structure and released STP hybridized to STP′ on the surface and dramatically disrupt the orientation of LCs mesogens.

2. Materials and methods

2.1. Materials and reagents

The standard glass microscope slides were purchased from HDA china. Copper grids (150 mesh, 165 μm pitch, and 20 μm in thickness), 4′-Pentyl-4-biphenylcarbonitrile (5CB) nematic liquid crystal 98 %, (3-aminopropyl)triethoxysilane (APTES) 99 %, and *N,N*-dimethyl-*N*-(3 (trimethoxysilyl) propyl)-1 octadecanaminiuchloride (DMOAP) 72 %, 3,3′,4,4′-Tetrachlorobiphenyl(PCB77), bisphenol A (BPA) 99 %, were provided by Sigma-Aldrich. Naphthalene 99 %, 4,4′-biphenol 97 %, 1,2-diphenylhydrazine, and benzyl butyl phthalate (BBP) 98 % standards were obtained from Merck.

The DNA sequences were synthesized and purified by using reverse-phase (RP) high performance liquid chromatography with the sequences as follows:

STP: 5′-AGA GAG AGA GAG AG-3′

STP′: 5′-C_6-Amine-CTC TCT CTC TCT CT-3′

PCB77 aptamer: 5′-CTC TCT GGC GGG GCT ACG AAG TAG TGA TTT TTT CCG ATG GCC CGT GTC TCT C-3′ (Mehta et al., 2012).

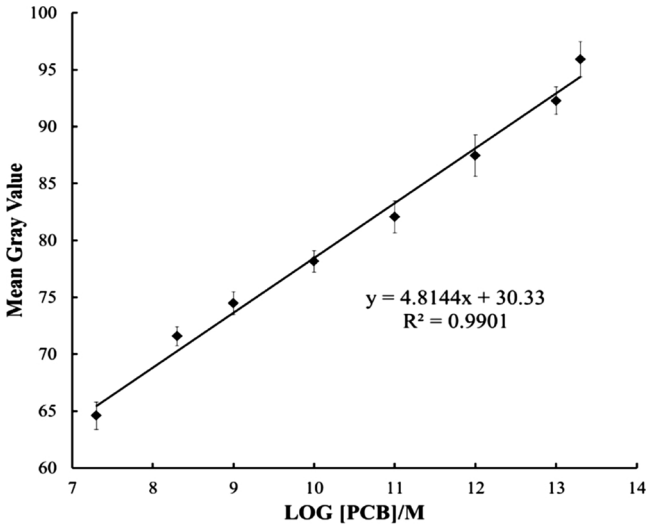

Fig. 3. Graph representing average grayscale intensity of the POM micrographs as a function of PCB77 concentration (n = 3).

The following sequences were dissolved in a Tris-HCl buffer (pH 7.6) containing 100 mM NaCl, 2 mM $MgCl_2$, 5 mM KCl, and 1 mM $CaCl_2$. Glutaraldehyde solution (GA) 50 %, glycine 99 %, acetonitrile 99.98 %, sulfuric acid 99.9 %, sodium dodecyl sulfate (SDS), and hydrogen peroxide 30 %, obtained Sigma-Aldrich.

2.2. Instruments

The LC optical cells were imaged under a polarized light microscope (Olympus BH2-UMA) in a transmission mode equipped with a crossed polarizer. All LC images were acquired by a digital camera (KECAM) affixed to the polarized light microscope. AFM (JPK-NanoWizard II) was performed to measure the topography of substrates. The AFM images were obtained in the contact mode with a scan rate of 1.2 Hz and scanning scope of 100 μm × 100 μm and 1 μm × 1 μm.

2.3. Cleaning of glass substrates

The glass slides substrates were cleaned in fresh prepared piranha solution (30 % H_2O_2 and 70 % H_2SO_4) at 80 ˚C thermostat water bath about 2 h, and were then rinsed several times with HPLC-grade water and ethanol, blew dry with nitrogen and drying in thermostat oven at 110 ˚C for 3 h before modification.

2.4. Slides preparation of the LC aptasensor

2.4.1. Preparation of DMOAP-treated substrate

The cleaned glass substrates were immersed in an aqueous solution of 0.35 % (v/v) DMOAP for 30 min at RT and then rinsed several times with ethanol and ultra-pure water respectively. Finally, The DMOAP-treated substrate was dried under tiny flow of nitrogen and was kept in a 110 ˚C oven for an hour. The DMOAP-decorated glass slides were then used as top substrate in the LC-based aptasensor.

2.4.2. Preparation of DMOAP/APTES-treated substrate

The cleaned glass slides were immersed in ethanol solution containing 3 % (v/v) APTES and 0.3 % (v/v) DMOAP at 80 ˚C for 2 h, then rinsed with ethanol and water, respectively and baked at 110 ˚C for 1 h after drying under nitrogen stream.

2.5. Immobilization of STP′ aptamers on DMOAP/APTES -treated substrate

To immobilize the STP′ linkers from amines terminals on the aptasensor, DMOAP/APTES -Treated substrate were immersed in 0.5 % (v/v) GA water solution at RT for 45 min, washed with HPLC-grade water, and dried under N_2.

Then the glass/DMOAP/APTES/GA substrate were immersed in the STP′ aptamer solution (200 μL, 100 nM, prepared with Tris-HCl buffer (pH 7.6) containing 100 mM NaCl, 2 mM $MgCl_2$, 5 mM KCl, and 1 mM $CaCl_2$), and incubated two hour at 37 ˚C and then rinsed with aptamer cleaning buffer and deionized water and dried under N_2.

After that, the modified substrate rinsed with a solution included of 0.3 M sodium chloride/0.03 M trisodium citrate containing SDS 0.01 %

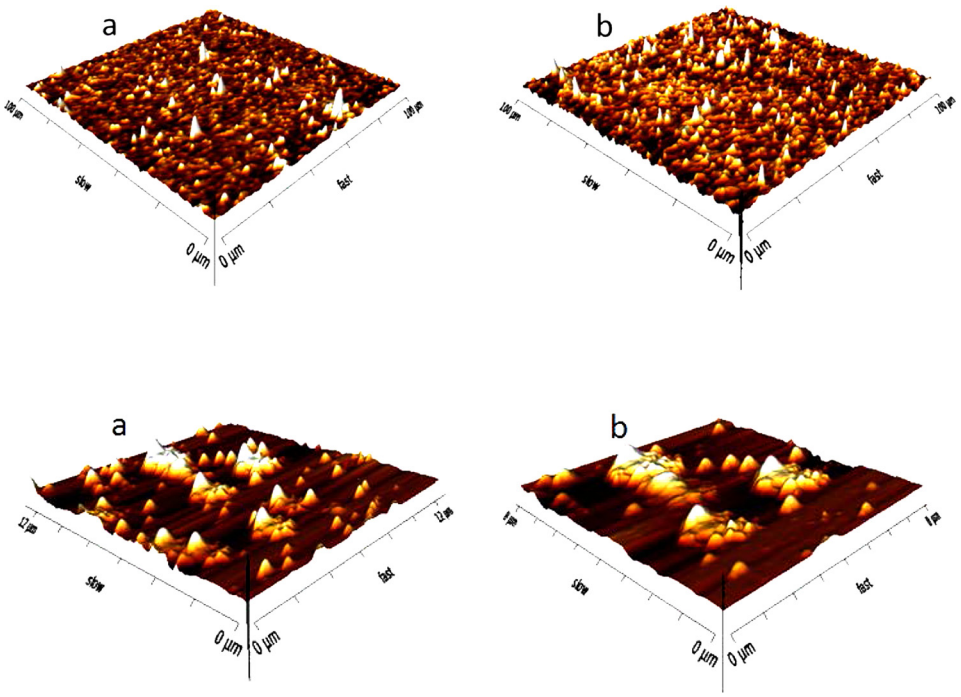

Fig. 4. (a) AFM three-dimensional images after assembling 100 nM STP′; (b) upon addition of THMS + PCB77 (1.5 μg/L); upper and lower images in scanning scope 100 × 100 μm and 1 × 1 μm, respectively.

Table 1
Comparison of the reported aptasensors for the PCB77 detection with presented LC aptasensor.

Detection Method	Strategy	Practical Samples	LOD (μg/L)	Linear range (μg/L)	Selectivity aganist	Selectivity results (Fig. S9)	Ref.
Colorimetric	salt-induced aggregation of AuNPs	real water	1.5 × 10^{-2}	1.5 × 10^{1} to 2.6 × 10^{2}	PCB72, PCB101, PCB126 naphthalen, pyrene, atrazine, bisphenol A, humic acid	the aptamer had little or no significant response to other contaminants	Cheng et al. (2018)
SERS	aptamer modified silica Au/core-shell nanoparticles	–	3 × 10^{2}	3 × 10^{2} to 5.8 × 10^{3}	PCB35, PCB47, PCB101	the aptamr modied SERS substrat demontrate desired sensing specici y to PCB77	Lu et al. (2014)
SERS	aptamer modified Ag-nanorod arrays	real lake water	9.6 × 10^{1}	9.6 × 10^{1} to 3 × 10^{2}	PCB3, PCB5, PCB28 PCB52, PCB101	the changes of Raman intensity ratios of for PCB77 is significantly stronger than that of other PCBs	Sun et al. (2016)
SERS	aptamer capturing in a microfluidic device	–	3	3 to 3 × 10^{4}	PCB5, PCB15,	the SERS spectrum of PCB77 was much stronger than that of PCB15 and PCB5	Fu et al. (2015)
Electrochemical	target-induced conformational changes of aptamer	tap water	3 × 10^{-5}	1 × 10^{-2} to 1 × 10^{1}	Hexachlorobenzene, PCB81, PCB126, PCB189	the signal of PCB77 shows the most significant change among the tested chemicals	Liang et al. (2019)
Electrochemical	multi-metal ions encoded nanospherical brushes	fish	3 × 10^{-4}	1 × 10^{-3} to 1 × 10^{1}	Kanamycin, streptomycin, PCB101, PCB28	similar compounds showed almost negligible responses current	Yan et al. (2015)
Photoelectrochemical	target-induced release of the DNA-CdS QDs probe	tap water and domestic sewage	1 × 10^{-4}	1 × 10^{-4} to 1 × 10^{-1}	PCB101, biphenyl, bisphenol A, benzopyrene, 17β-estradiol, atrazine	PCB101 had 29.4 % $\Delta I_u/\Delta I_0$ signal	Fan et al. (2019)
Photoelectrochemical	target-induced complex formation and inhibited the electron transfer	environmental water sample	4.4	1 × 10^{1} to 1 × 10^{3}	Oxytetracycline, Ofloxacin, p Nitrophenol, Bisphenol A, Hydroquinone, Cd^{2+}, Hg^{2+}, Cu^{2+}, Zn^{2+}, Fe^{2+}, Co^{2+}, PCB7, PCB77	all these species do not induce obvious deflection of detection signal	Yan et al. (2018)
Liquid crystal	THMS and duplex-induced homeotropic to tilted transition	tap water, environmental water and milk	1.5 × 10^{-5}	1.5 × 10^{-5} to 1.5 × 10^{1}	benzyl butyl phthalate, bisphenol A, naphthalene, 4,4′-biphenol, 1,2-diphenylhydrazine	similar chemicals could not disturb the ordered alignment of LC molecules	In this study

Fig. 5. Optical appearances of the LC cells under crossed polarizers with different interferer molecules: BBP, bisphenol A, naphthalene, 4,4′-biphenol and 1,2-diphenylhydrazine.

Table 2
Recovery of PCB77 from real samples (n = 4). Data are mean with relative standard deviation (RSD).

Samples	Added (μg/L)	Found (μg/L)	Recovery (%)	RSD (%, n = 4)
Tap water 1	0.0007	0.00068	93.72	12.9189
Tap water 2	0.0015	0.0015	100.50	3.0505
Tap water 3	0.0029	0.0030	103.78	12.4645
Tap water 4	0.0292	0.02984	102.15	5.7788
Tap water 5	0.292	0.2976	101.92	5.0664
Tap water 6	0.584	0.5932	101.57	8.7021
Tap water 7	1.46	1.4057	96.28	0.8519
Lake water 1	0.0007	0.0008	110.06	17.4365
Lake water 2	0.0015	0.0014	97.38	8.4375
Lake water 3	0.0029	0.0025	87.89	21.2143
Lake water 4	0.0292	0.032	109.76	6.9128
Lake water 5	0.292	0.2773	94.98	6.4688
Lake water 6	0.584	0.6167	105.60	1.8239
Lake water 7	1.46	1.4569	99.78	16.4513
Milk 1	0.0007	0.0008	102.42	3.9631
Milk 2	0.0015	0.00135	90.13	11.3210
Milk 3	0.0029	0.003	103.78	12.4645
Milk 4	0.0292	0.0269	92.11	10.1492
Milk 5	0.292	0.276	94.51	6.4688
Milk 6	0.584	0.574	98.26	6.0560
Milk 7	1.46	1.4485	99.21	8.1674

(v/v) and water to remove nonspecific interference. Finally, the glass/DMOAP/APTES/GA/aptamer substrates were treated with glycine solution (80 mM) for 1 h, rinsed with water and dried under tiny flow of nitrogen.

2.6. Preparation of triple-helix molecular switch

The THMS was prepared by mixing the aptamer (150 nM final concentration) and STP (150 nM final concentration) in buffer (Tris-HCl buffer (pH 7.6) containing 100 mM NaCl, 2 mM $MgCl_2$, 5 mM KCl, and 1 mM $CaCl_2$). The mixture was incubated at RT for 1 h.

200 μL different concentrations of PCB77 solution were incubated with THMS at 37 ˚C for 15 min. Subsequently, 100 μL injected onto the glass/DMOAP/APTES/GA/STP′-Treated substrate. The unbonded molecules on the surface were washed with 2 × SSC buffer (containing 0.1 % SDS) and ultra-pure water, finally dried under nitrogen stream. Subsequently, a copper grid (20 μm thickness) was first placed onto the glass/DMOAP/APTES/GA/STP′-treated substrate.

2.7. The fabrication process of the LC-cells

2 μL of 5CB (isotropic state at 40 ˚C) was spotted onto the copper grid and the excessive LCs removed by using a clean capillary tube. After that, the DMOAP-treated substrate was put onto assembled cell. It was sandwiched between two modified substrate, and secured with binder clips.

2.8. Analysis of the selectivity of the LC-based aptasensor

The specificity of the proposed LC-based platform was examined by POM image analysis of other similarly structured analogs, such as bisphenol A, naphthalene, 4,4′-biphenol, 1,2-diphenylhydrazine, and benzyl butyl phthalate (0.1 nM the concentration of each material) as mentioned before. Data are means ± SD, n = 4

2.9. Detection of PCB77 in real samples

2.9.1. Detection of real water sample

To investigate the application of the proposed LC-aptasensor in real water samples, tap water, and lake water samples used in this study. Lake samples were collected from the Jamab River, Mashhad, Iran. Before analyzing via the water samples, all samples were pre-treated filtered with a Whatman filter to eliminate the gross particles. Then, the samples were centrifuged at 12,000 *g* for 5 min, and the upper supernatant stacked up. Finally, the sample was passed several times through a 0.22 μm Millipore filter to remove the suspended matters. Different concentrations of the target molecule were spiked into filtered samples of water. After preparing the LC-cell according to the mentioned instruction and immobilizing the aptamers, 100 microliters of the real sample containing a certain concentration of PCB 77 was injected into the cell and after incubation for 15 min, the cell was washed with distilled water and the images were recorded.

2.9.2. Detection of milk sample

To reduce the interference of the complex milk matrix solution (fat content of 3.2 % (w/v)) during the detection, the milk samples were diluted 100 times with the ultra-pure water. The diluted milk sample and cold acetonitrile and (1:3) were gently mixed and incubated for 60 min at 4 ˚C to separate the milk proteins. The mixture was centrifuged at 9500 *g* for 15 min, and the supernatant was stacked up and preserved at 4 ˚C for subsequent assays. Then, the increasing concentrations of PCB77 were spiked to pretreated samples. After preparation of the LC-cell and immobilizing the aptamers, 100 microliters of the spiked milk sample was injected into the cell, and its recovered concentrations were recorded.

3. Results and discussions

3.1. Assembling of THMS structure and sensing platform

Scheme 1 illustrates the sensing strategy of the proposed LC aptasensor for PCB77 based on the THMS structure. The aptamer contained triple-helix molecular switch (THMS) is formed by pre-hybridization of a central, target-specific aptamer sequence (red) flanked by two terminal fragments (brown) with STP (in navy blue), is complementary of aptamer terminal fragments based on Hoogsteen and Watson-Crick base pairings. In the presence of PCB77, aptamer preferentially bind to the target, which disrupts the arrangement of the THMS. Thus, STP dissociates from the THMS and hybrids with STP′ on LC cell.

STP′ immobilized on the DMOAP/APTES-treated substrate via amide bonds between active aldehyde surface groups and amine-terminals of STP′ with GA as a crosslinking.

It has demonstrated that the alignment agents (such as DMOAP) induced the homeotropic orientation of 5CB. As we know, when the LC has a homeotropic orientation, light cannot pass through crossed analyzer, so a dark polarized light image appears. However, in the presence of PCB77, STP hybrids with the STP′ immobilized on the substrate and considerably disrupt the homeotropic orientation of LC molecules. As a result, the POM images of the 5CB change from dark to bright after hybridization (Scheme 1).

3.2. The performance of the sensing platform

As shown in Fig. 1a, a uniform dark image was recorded for the LC aptasensor when STP′ immobilized on LC-cell, indicating that STP′ could not disrupt the homeotropic alignment of LC mesogens. In the absence of PCB77 when the THMS added to the STP′ immobilized LC-cell, the change in the surface topology was very little and the POM background image remained dark Fig. 1b.

While, a great change in the surface topology happens by PCB77 and induce LCs to undergo homeotropic-to-tilted transition, causing birefringence in the optical image, as shown in Fig. 1c.

3.3. Optimiation of the chemical modifiers on the substrates

To provide long aliphatic chains favoring the vertical alignment of LC mesogens and active groups for the aptamer immobilization, DMOAP and APTES immobilized on the substrate, respectively. The ratio of these two silane agents on sensor substrates should be optimized to avoid background interference and reach to the maximum sensing efficiency.

Since the presences of APTES affect the fixation amount of aptamer, we choose two different percent of DMOAP with different DMOAP/APTES volume ratio (1:1, 1:2, 1:5 and 1:10).

Figs. S2 and S3 show the DMOAP/APTES volume ratios 1:5 and 1:1 are the optimal ratios in 1 % and 0.3 % of DMOAP, respectively, in which the homeotropic orientation of cylindrical shape LC molecules has been preserved.

We investigated various GA percent for the optimal APTES/DMOAP ratios. We found that the POM images were dark up to 0.5 % GA, irrespective of the DMOAP percent. In contrast, when the GA percent was above 0.5, the colored pixels began to appear in the POM images (Figs. S4 and S5), suggesting that a cross-linking reaction occurred between the APTES molecules and disrupted the orientation of LC films.

Similarly, the amount of STP′ can affect the surface density of LC layer. We immobilize 50–300 nM concentrations of STP′ as the capture probe with optimal concentrations of modifier agents on the sensing platform.

As shown in Fig. S6, the bright colored areas were observed in POM images in 1 % of DMOAP with 1:5 APTES/DMOAP ratios, indicating that the orientation of the LC layer was highly affected by STP′ amount.

In contrast, in 0.3 % of DMOAP with 1:1 APTES/DMOAP ratio up to 100 nM STP′ a uniformly dark background of the LC POMs achieved (Fig. S7).

Based on these results, we chose the 1 % DMOAP with DMOAP/APTES 1:1 vol ratio, 0.5 % GA and 100 nM STP′ as the optimal parameters for the assembling of our LC-based aptasensor.

3.4. Detection of PCB77 by LC-based aptasensor

To confirmation of the proposed aptsensor feasibility, we investigated the LC aptasensor POMs in different concentrations of PCB77.

A homeotropic orientation and uniform dark POMs were observed at CPCB77 = 0 μg/L (Fig. 2a). In contrast, A few bright patches appeared at CPCB77 = 1.5×10^{-5} μg/L (Fig. 2b) and a complete homeotropic-to-tilted transition were observed at CPCB77 ≥ 15 μg/L (Fig. 2i).

Hence, the captured STP on the surface of LC cell could be disrupting the LC-decorated monolayer, thereby inducing a change of the optical response from 1.5×10^{-5} μg/L to 15 μg/L of PCB77. The

corresponding 3D surface plot of LCs images associated with the concentrations of PCB77 was given in Fig. S8.

In addition, there is a good linear relationship between the average gray-scale intensities (GIs) of the POMs and the logarithm of PCB77concentrations (using the ImageJ free software), presented in Fig. 3.

Quantification analysis of the POMs, reveals that the LC-based aptasensor can detect the PCB77 through the changes of POMs from dark to bright in the range from 1.5×10^{-5} μg/L to 15 μg/L with the limit of quantification 1.5×10^{-5} μg/L.

The atomic force microscope (AFM) images (Fig. 4a) indicates that the assembled STP′ layer possesses an almost uniform surface microstructure. In contrast, in the present of PCB77 the liberated STP from THMS structure can well hybridize with the STP′, and causing the tilted orientation of LC molecules. Therefore, the corresponding AFM image showed that the topographical structure changed considerably (Fig. 4b).

The results support the assumption that binding PCB77 and the recognition aptamer disrupted THMS and, the duplex formation changed the surface topography.

To prove the sensitivity of LC-based aptasensor, we compared our work with other previously reported aptasensors for the detection of PCB77, as shown in Table 1. These approaches try to improve the binding affinity of PCB77 aptamer (GGC GGG GCT ACG AAG TAG TGA TTT TTT CCG ATG GCC CGT G) including the optimization of various conditions such as buffer, ions, pH, temperature, stabilization of aptamer structures, the accessible surface area, conjugation of binding motifs, and use amplifier signal agents such as nanomaterials.

The ultra-low detection limit of PCB77 of the LC-based aptasensor is found to be 1.5×10^{-5} μg/L, which is well below the other reported LODs. On the other hand, we do not need sophisticated and expensive devices in this detection assay.

3.5. The specificity of monitoring PCB77

Basically, a LCs-based sensing platform must be highly specific toward its analyte for practical applicability. Therefore, to further confirm the feasibility of PCB77 detection, we tested the LC-based aptasensor with similar chemical analogs. As can be seen in Fig. 5, bisphenol, naphthalene, 4,4′-biphenol, 1,2-diphenylhydrazine, and BBP having no specific binding to the PCB77 aptamer. Therefore, similar chemicals could not disturb the ordered alignment of LC molecules, indicating that the LC-based aptasensor has a good selectivity to PCB77.

3.6. Real sample analysis

After verifying the performance of the LC-based aptasensor for sensing PCB77, we tried to investigate recoveries of the spiked real samples including, tap water, environmental water and milk. The analytical results in Table 2 indicate the recoveries are between 92.11 % and 110.06 %. It indicating good accuracy of the proposed LC- based aptasensor for the PCB77 detection. The real sample analysis suggested that this new LC aptasensing platform for PCB77 detection was reliable and feasible for food safety, and environmental sample analysis.

4. Conclusions

In summary, we developed a novel molecular engineering strategy as a universal LC-based sensing platform for the long-sequence aptamers based on a THMS structure. We studied optical behavior of LC cell in the present of target under the polarized microscope. We choose PCB77 as a proof-of-concept model owing to its toxic effects on health and food safety threat. The detection mechanism is based on specific binding of PCB77 to the aptamer and duplex forming on the LCs cell, which alters considerably the homeotropic orientation of LC. As a result, the POM images of the 5CB shift from dark to bright in the range of 1.5×10^{-5} to 15 μg/L. The limit of quantification the ultra-sensitive developed LC aptasensor was 1.5×10^{-5} μg/L. Besides, we also showed that this aptasensor could be applied in real samples such as tap water, environmental water and milk. Our approach offers the opportunity to overcoming many challenges of LC-aptsensors for different analytes as an easy-to-operate, ultra-sensitive, and portable assay.

CRediT authorship contribution statement

Asma Verdian: Conceptualization, Methodology, Writing - original draft, Writing - review & editing. **Zeinab Rouhbakhsh:** Investigation, Software. **Ebrahim Fooladi:** Investigation.

Declaration of Competing Interest

The author(s) declare that they have no competing interests.

Acknowledgements

This work was financed by the Iran National Science Foundation (INSF) as a project (Project 96006484) and supported by the Research Institute of Food Science and Technology (RIFST).

Appendix A. Supplementary data

Supplementary material related to this article can be found, in the online version, at doi:https://doi.org/10.1016/j.jhazmat.2020.123531.

References

Ahmad, I., Weng, J., Stromberg, A., Hilt, J., Dziubla, T., 2019. Fluorescence based detection of polychlorinated biphenyls (PCBs) in water using hydrophobic interactions. Analyst 144, 677–684.
Alver, A., Baştürk, E., 2019. Removal of Aspartame by Catalytic Ozonation with Nano-TiO_2 Coated Pumice.
Alver, A., Kılıç, A., 2018. Catalytic ozonation by iron coated pumice for the degradation of natural organic matters. Catalysts 8, 219.
Alver, A., Baştürk, E., Kılıç, A., 2018. Disinfection by-products formation potential along the Melendiz River, Turkey; associated water quality parameters and non-linear prediction model. Int. J. Environ. Res. 12, 909–919.
Argun, M.E., Alver, A., Karatas, M., 2017. Optimization of landfill leachate oxidation at extreme conditions and determination of micropollutants removal. Desalin. Water Treat. 90, 130–138.
Bagheri, E., Abnous, K., Alibolandi, M., Ramezani, M., Taghdisi, S.M., 2018. Triple-helix molecular switch-based aptasensors and DNA sensors. Biosens. Bioelectron. 111, 1–9.
Berger, U., Herzke, D., Sandanger, T.M., 2004. Two trace analytical methods for determination of hydroxylated PCBs and other halogenated phenolic compounds in eggs from Norwegian birds of prey. Anal. Chem. 76, 441–452.
Carpenter, D.O., 2006. Polychlorinated biphenyls (PCBs): routes of exposure and effects on human health. Rev. Environ. Health 21, 1–24.
Cheng, R., Liu, S., Shi, H., Zhao, G., 2018. A highly sensitive and selective aptamer-based colorimetric sensor for the rapid detection of PCB 77. J. Hazard. Mater. 341, 373–380.
Chiu, Y.-W., Li, Q.X., Karu, A.E., 2001. Selective binding of polychlorinated biphenyl congeners by a monoclonal antibody: analysis by kinetic exclusion fluorescence immunoassay. Anal. Chem. 73, 5477–5484.
Choi, S.M., Yoo, S.D., Lee, B.M., 2004. Toxicological characteristics of endocrine-disrupting chemicals: developmental toxicity, carcinogenicity, and mutagenicity. J. Toxicol. Environ. Health Part B 7, 1–23.
Clemente, A.P.B., Kuang, H., Shabana, A.M., Labuza, T.P., Kokkoli, E., 2019. Design of an aptamer-amphiphile for the detection of β-lactoglobulin on a liquid crystal interface. Bioconjug. Chem. 30 (11), 2763–2770.
Du, J., Jiang, Q., Lu, X., Chen, L., Zhang, Y., Xiong, X., 2019. Detection of sulfadimethoxine using optical images of liquid crystals. Analyst 144, 1761–1767.
Fan, L., Zhang, C., Shi, H., Zhao, G., 2019. Design of a simple and novel photoelectrochemical aptasensor for detection of 3, 3′, 4, 4′-tetrachlorobiphenyl. Biosens. Bioelectron. 124, 8–14.
Fu, C., Wang, Y., Chen, G., Yang, L., Xu, S., Xu, W., 2015. Aptamer-based surface-enhanced Raman scattering-microfluidic sensor for sensitive and selective polychlorinated biphenyls detection. Anal. Chem. 87, 9555–9558.
Hu, M., Yang, H., Li, Z., Zhang, L., Zhu, P., Yan, M., Yu, J., 2020. Signal-switchable lab-on-paper photoelectrochemical aptasensing system integrated triple-helix molecular switch with charge separation and recombination regime of type-II CdTe@ CdSe core-shell quantum dots. Biosens. Bioelectron. 147, 111786.
Hussain, Z., Qazi, F., Ahmed, M.I., Usman, A., Riaz, A., Abbasi, A.D., 2016. Liquid crystals based sensing platform-technological aspects. Biosens. Bioelectron. 85, 110–127.

Javidi, M., Housaindokht, M.R., Verdian, A., Razavizadeh, B.M., 2018. Detection of chloramphenicol using a novel apta-sensing platform based on aptamer terminal-lock in milk samples. Anal. Chim. Acta 1039, 116–123.
Khoshbin, Z., Verdian, A., Housaindokht, M.R., Izadyar, M., Rouhbakhsh, Z., 2018. Aptasensors as the future of antibiotics test kits-a case study of the aptamer application in the chloramphenicol detection. Biosens. Bioelectron. 122, 263–283.
Khoshbin, Z., Housaindokht, M.R., Izadyar, M., Verdian, A., Bozorgmehr, M.R., 2019. A simple paper-based aptasensor for ultrasensitive detection of lead (II) ion. Anal. Chim. Acta 1071, 70–77.
Kim, H.J., Jang, C.-H., 2019. Liquid crystal-based aptasensor for the detection of interferon-γ and its application in the diagnosis of tuberculosis using human blood. Sens. Actuators B: Chem. 282, 574–579.
Kim, H., An, Z., Jang, C.-H., 2018. Label-free optical detection of thrombin using a liquid crystal-based aptasensor. Microchem. J. 141, 71–79.
Knerr, S., Schrenk, D., 2006. Carcinogenicity of "non-dioxinlike" polychlorinated biphenyls. Crit. Rev. Toxicol. 36, 663–694.
Liang, S., Wu, L., Liu, H., Li, J., Chen, M., Zhang, M., 2019. Organic molecular passivation of phosphorene: an aptamer-based biosensing platform. Biosens. Bioelectron. 126, 30–35.
Lu, Y., Huang, Q., Meng, G., Wu, L., Jingjing, Z., 2014. Label-free selective SERS detection of PCB-77 based on DNA aptamer modified SiO 2@ Au core/shell nanoparticles. Analyst 139, 3083–3087.
Mehta, J., Rouah-Martin, E., Van Dorst, B., Maes, B., Herrebout, W., Scippo, M.-L., Dardenne, F., Blust, R., Robbens, J., 2012. Selection and characterization of PCB-binding DNA aptamers. Anal. Chem. 84, 1669–1676.
Nandi, R., Pal, S.K., 2018. Liquid crystal based sensing device using a smartphone. Analyst 143, 1046–1052.
Ozcan, S., Tor, A., Aydin, M.E., 2009. Determination of selected polychlorinated biphenyls in water samples by ultrasound-assisted emulsification-microextraction and gas chromatography-mass-selective detection. Anal. Chim. Acta 647, 182–188.
Popov, P., Mann, E.K., Jákli, A., 2017. Thermotropic liquid crystal films for biosensors and beyond. J. Mater. Chem. B 5, 5061–5078.
Qi, L., Hu, Q., Kang, Q., Bi, Y., Jiang, Y., Yu, L., 2019. Detection of biomarkers in blood using liquid crystals assisted with aptamer-target recognition triggered in situ rolling circle amplification on magnetic beads. Anal. Chem. 91, 11653–11660.
Ren, H., An, Z., Jang, C.-H., 2019. Liquid crystal-based aptamer sensor for sensitive detection of bisphenol a. Microchem. J. 146, 1064–1071.
Robertson, L.W., Hansen, L.G., 2015. PCBs: Recent Advances in Environmental Toxicology and Health Effects. University Press of Kentucky.
Rouhbakhsh, Z., Verdian, A., Rajabzadeh, G., 2020. Design of a liquid crystal-based aptasensing platform for ultrasensitive detection of tetracycline. Talanta 206, 120246.
Safe, S.H., 1994. Polychlorinated biphenyls (PCBs): environmental impact, biochemical and toxic responses, and implications for risk assessment. Crit. Rev. Toxicol. 24, 87–149.
Shen, J., He, F., Chen, L., Ding, L., Liu, H., Wang, Y., Xiong, X., 2017. Liquid crystal-based detection of DNA hybridization using surface immobilized single-stranded DNA. Microchim. Ichnoanal. Acta 184, 3137–3144.
Steel, A., Levicky, R., Herne, T., Tarlov, M.J., 2000. Immobilization of nucleic acids at solid surfaces: effect of oligonucleotide length on layer assembly. Biophys. J. 79, 975–981.
Sun, K., Huang, Q., Meng, G., Lu, Y., 2016. Highly sensitive and selective surface-enhanced Raman spectroscopy label-free detection of 3, 3′, 4, 4′-tetrachlorobiphenyl using DNA aptamer-modified Ag-nanorod arrays. ACS Appl. Mater. Interfaces 8, 5723–5728.
Tan, H., Li, X., Liao, S., Yu, R., Wu, Z., 2014. Highly-sensitive liquid crystal biosensor based on DNA dendrimers-mediated optical reorientation. Biosens. Bioelectron. 62, 84–89.
Verdian, A., 2018. Apta-nanosensors for detection and quantitative determination of acetamiprid–a pesticide residue in food and environment. Talanta 176, 456–464.
Verdian, A., Housaindokht, M.R., Abnous, K., 2014. A fluorescent aptasensor for potassium ion detection-based triple-helix molecular switch. Anal. Biochem. 466, 72–75.
Verdian, A., Fooladi, E., Rouhbakhsh, Z., 2019. Recent progress in the development of recognition bioelements for polychlorinated biphenyls detection: antibodies and aptamers. Talanta 202, 123–135.
Wang, Y., Wang, B., Shen, J., Xiong, X., Deng, S., 2017. Aptamer based bare eye detection of kanamycin by using a liquid crystal film on a glass support. Microchim. Ichnoanal. Acta 184, 3765–3771.
Yan, Z., Gan, N., Wang, D., Cao, Y., Chen, M., Li, T., Chen, Y., 2015. A "signal-on"aptasensor for simultaneous detection of chloramphenicol and polychlorinated biphenyls using multi-metal ions encoded nanospherical brushes as tracers. Biosens. Bioelectron. 74, 718–724.
Yan, K., Zhu, Y., Ji, W., Chen, F., Zhang, J., 2018. Visible light-driven membraneless photocatalytic fuel cell toward self-powered aptasensing of PCB77. Anal. Chem. 90, 9662–9666.
Yang, S., Wu, C., Tan, H., Wu, Y., Liao, S., Wu, Z., Shen, G., Yu, R., 2012. Label-free liquid crystal biosensor based on specific oligonucleotide probes for heavy metal ions. Anal. Chem. 85, 14–18.
Zarei, M., 2017. Portable biosensing devices for point-of-care diagnostics: recent developments and applications. TrAC Trends Anal. Chem. 91, 26–41.
Zhang, H., Zhou, L., Zhu, Z., Yang, C., 2016. Recent progress in aptamer-based functional probes for bioanalysis and biomedicine. Chem. Eur. J. 22, 9886–9900.
Zheng, J., Li, J., Jiang, Y., Jin, J., Wang, K., Yang, R., Tan, W., 2011. Design of aptamer-based sensing platform using triple-helix molecular switch. Anal. Chem. 83, 6586–6592.